People's Democratic Republic of Algeria
Ministery of Higher Education and Scientific Research
Mohamed El Bachir El Ibrahimi University of Borj Bou Arrerij
Faculty of Mathematics and Informatics
Informatics Department

DISSERTATION

Presented in fulfillment of the requirements of obtaining the degree

Master in Informatics

Specialty: Business Intelligence

THEME

Brain Tumor Detection Using U-Net and SVM

Presented by:

BENGUEZZOU Mohammed

BENYAHIAOUI Mohamed Assil

Publicly defended on: jj/mm/aaaa

In front of the jury composed of:

President: .....

Examiner: .....

Supervisor: Dr. ZOUAOUI Hakima

2024/2025

Dedication

To the architects of my dreams, my parents, whose unwavering love and guidance have been my compass; to my family, the sanctuary of my heart, and to my friends, the sparks of joy in my journey.

This thesis is a testament to your belief in me, a reflection of your sacrifices, and a celebration of the bond we share. Thank you for being my pillars of strength and my endless source of inspiration.

- Mohammed

Dedication

To my parents, whose unwavering love, support, and guidance have been instrumental in shaping my dreams; to my family, who have been my rock and my safe haven; and to my friends, who have been the source of joy and laughter in my life.

This thesis is a reflection of their sacrifices, a testament to their faith in me, and a celebration of the bond we share. Thank you for being my pillars of strength and my endless source of inspiration.

- Assil

Ackowledgments

Above all, we would like to thank GOD for granting health, the possibility and the will to start and continue our studies.

We would first like to thank to our supervisor, **Dr. Hakima Zouaoui**, forgiving us the chance to do our research and for providing invaluable guidance throughout this research. Also, we would acknowledge her for her generosity, her kindness, her knowledge, the time she gave us and her great availability which she showed us; made our task a lot easier.

We would also like to express our thanks to the members of the jury whohonored us by participating in the examination of this work and enrichin git with their proposals **Dr. !!!!!!!** and **Dr. !!!!!!!**.

In addition, we would like to acknowledge our parents for their love, care, prayers, scarifies and for being always there for us

Abstract

Brain tumors, particularly gliomas, pose a significant clinical challenge, requiring both precise localization and accurate grading to guide treatment. Accurate segmentation of tumor regions is a critical first step, enabling meaningful analysis and interpretation of the affected areas. In this project, we present a hybrid framework that first segments tumor regions in brain Magnetic Resonance Imaging (MRI) scans using a U-Net model trained on the Brain Tumor Segmentation dataset, and then classifies these regions as Low-Grade or High-Grade Gliomas with a Support Vector Machine (SVM) model based on features extracted from the segmented masks. On the held-out test set, our U-Net achieved an accuracy of 99.3%, while the SVM classifier delivered an overall accuracy of 93%.

Keywords: Brain Tumor, U-Net, SVM, MRI, BraTS, Segmentation.

Résumé

Les tumeurs cérébrales, en particulier les gliomes, posent un défi clinique important, nécessitant à la fois une localisation précise et un classement précis pour guider le traitement. La segmentation précise des régions tumorales est une première étape essentielle, permettant une analyse et une interprétation significatives des zones touchées. Dans ce projet, nous présentons un cadre hybride qui segmente d'abord les régions tumorales dans l'imagerie par résonance magnétique (IRM) du cerveau en utilisant un modèle U-Net formé sur le jeu de données de segmentation des tumeurs cérébrales, puis classe ces régions comme faibleGliomes de grade ou de haut grade avec un modèle SVM (Support Vector Machine) basé sur les caractéristiques extraites des masques segmentés. Sur l'ensemble de test non exécuté, notre U-Net a atteint une précision de 99,3

Mots-clés: Tumeur cérébrale, U-Net, SVM, IRM, BraTS, Segmentation.

ملخص

تُشكل أورام الدماغ، وخاصة الأورام الدبقية، تحديا طبيا كبيراً، وتتطلب الى التحديد والتصنيف بشكل دقيق من أجل توجيه العلاج. إن التقسيم الدقيق لمناطق الورم يعد خطوة أولى بالغة الأهمية، حيث يتيح إجراء تحليل وتفسير مفيد للمناطق المصابة. في هذا المشروع، نقدم إطاراً هجينا يقوم أولاً بتقسيم مناطق الورم في عمليات مسح (MRI) للدماغ باستخدام نموذج (U-Net) المدرب على مجموعة بيانات أورام الدماغ (BraTS2020) ثم يقوم بتصنيف هذه المناطق على أنها أورام دبقيه منخفضة الدرجة أو عالية الدرجة باستخدام نموذج آلة الدعم المتجه (SVM) استناداً إلى الميزات المستخرجة من الأقنعة المجزأة. في مجموعة الاختبار، حققت شبكة (U-Net) الخاصة بنا دقة قدرها 99,3%، بينما قدم مصنف (SVM) دقة إجمالية قدرها 93%.

الكلمات المفتاحية: اورام الدماغ، U-Net، SVM، MRI، BraTS، Segmentation.

Table of Contents

List of abbreviations

AI Artificial Intelligence.

CNN Convolutional Neural Network.

CNS Central Nervous System.

CT Computed Tomography.

ML Machine Learning.

MRI Magnetic Resonance Imaging.

NADE Neural Autoregressive Distribution Estimator.

RNN Recurrent Neural Network.

SVM Support Vector Machine.

U-Net U-Net Convolutional Neural Network.

WHO World Health Organization.

List of Figures

List of Tables

General Introduction

Traditionally, radiologists rely on MRI scans to detect brain tumors, While this method is effective, it also has limitations analyzing hundreds of scans manually is time consuming and prone to human error. That is where technology comes in. With recent advances in artificial intelligence, especially deep learning, we now have powerful tools that can learn from medical images and help with faster and more accurate diagnosis.

In this project, we focus on building a hybrid system to detect brain tumors and determine whether they are low-grade or high-grade. We use a U-Net model for segmenting the tumor regions in MRI images. After identifying these regions, we extract important features and feed them into a Support Vector Machine (SVM) classifier to make the final prediction.

We use the BraTS2020 dataset, focusing on T2-weighted FLAIR images, to train and test our system. Our goal is to create a pipeline that is not only technically sound but also practical and helpful for medical professionals in real-world settings.

Chapter 1

Medical and Technical Concepts

1.1 Introduction

This chapter provides essential background information on the clinical and technological context of the thesis. We begin by describing the brain and its tissues from both macroscopic and microscopic perspectives. We then discuss brain tumors, which are the primary focus of this research. Next, we introduce the different types of medical imaging modalities and explain the importance of segmentation tasks in neuro-oncology. Finally, we delve deeper into the principles and components of Magnetic Resonance Imaging (MRI), which is the primary imaging modality used in this thesis.

1.2 Macroscopic and Microscopic Description of the Brain

1.2.1 Macroscopic Description

The human brain is an irregular, ovoid organ with a large anteroposterior axis. Its average volume is approximately 1100 cm^3 in women and 1400 cm^3 in men, and it weighs between 1400 g and 1800 g. It occupies the cranial cavity but does not contact the bone directly, as it is suspended in cerebrospinal fluid inside a fluid chamber [5].

The brain comprises four main regions: the cerebrum, cerebellum, brainstem, and diencephalon (Figure 1.1).

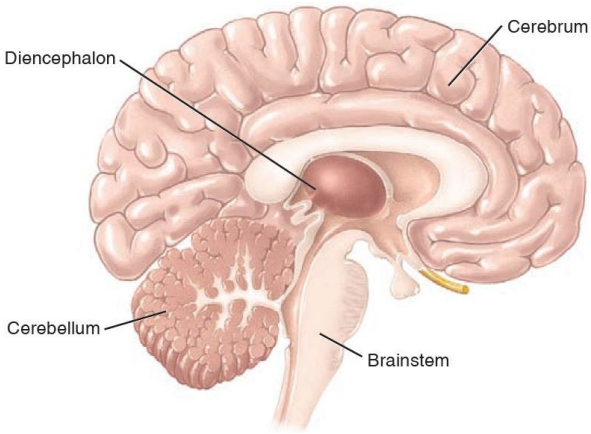

Figure 1.1: Brain main parts: cerebrum, cerebellum, brainstem, and diencephalon [1].

1.2.1.1 Cerebrum

The cerebrum is the largest part of the brain, representing about 83% of its total volume. It is divided into right and left hemispheres connected by the corpus callosum. Each hemisphere controls the contralateral side of the body (Figure 1.2).

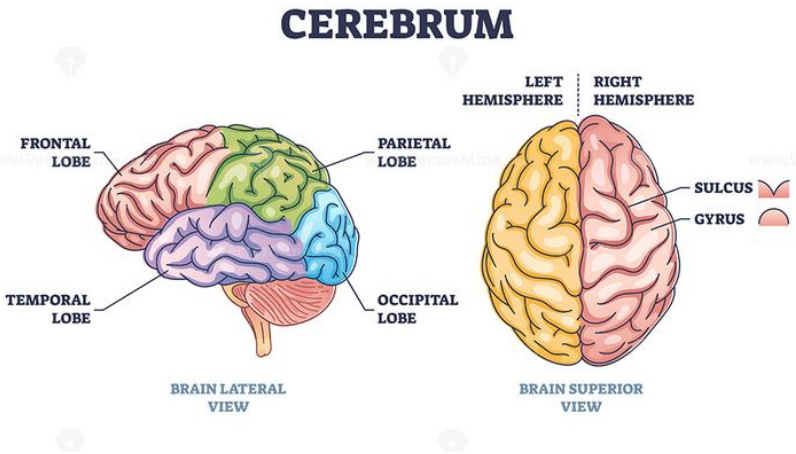

Figure 1.2: Cerebrum brain structure from lateral and superior view outline diagram.[1].

Each hemisphere contains four lobes—frontal, parietal, occipital, and temporal—with distinct functions (Figure 1.2).

Frontal lobes

- Speech, language, reasoning, decision-making, personality, judgment, and voluntary movements.
- Right frontal lobe controls left-side movements; left frontal lobe controls right-side move-

ments.

Parietal lobes

- Reading, spatial and visual perception, touch, pain, and temperature sensation.
- Right parietal lobe mediates left-side sensitivity; left parietal lobe mediates right-side sensitivity.

Occipital lobes

- Visual processing (color, light, movement).

Temporal lobes

- Language comprehension, memory, and emotion processing.
- Sequencing and organization.

1.2.1.2 Cerebellum

The cerebellum lies below the cerebrum and accounts for about 11% of brain volume. It coordinates reflexes, movement, balance, and posture.

1.2.1.3 Brainstem

The brainstem connects the cerebrum and cerebellum to the spinal cord and controls vital functions such as eye movements, breathing, blood pressure, and heart rate.

1.2.1.4 Diencephalon

Surrounded by the cerebral hemispheres, the diencephalon coordinates motor functions, maintains consciousness, regulates autonomic functions (eating, thirst, temperature, circadian rhythm) and interacts with both brain and cerebellum [6].

1.2.2 Microscopic Description

From a microscopic point of view, the nervous tissue consists of nerve cells (neurons) and glial cells (support and protective cells) that derive from the ectoderm. Vessels and meninges

do not belong to the nervous tissue and are derived from the mesoderm. The neuron is the cell that constitutes the functional unit of the neuroaxis. Neurons are 10 to 50 times more numerous than glial cells. The human nervous system comprises about 100 billion neurons. Neurons transmit a signal or what we call nerve impulses [5].

1.3 Brain Tissue

Accurate segmentation of brain tissues in MRI is critical for diagnosis and treatment planning. Anatomical structures can be divided into hemispheres and lobes, but for imaging, we often classify voxels as gray matter, white matter, or cerebrospinal fluid [7].

1.3.1 Gray Matter

Gray matter contains neuronal cell bodies (soma), axon tracts, glial cells, capillary blood vessels, and neuropil (dendrites, unmyelinated axons, glia) [8].

1.3.2 White Matter

White matter consists primarily of myelinated axons (tracts), oligodendrocytes, and astrocytes, forming the brain's long-range connections [8].

1.3.3 Cerebrospinal Fluid

Cerebrospinal fluid (CSF) cushions the brain and spinal cord, removes metabolic waste, and maintains proper central nervous system function [9].

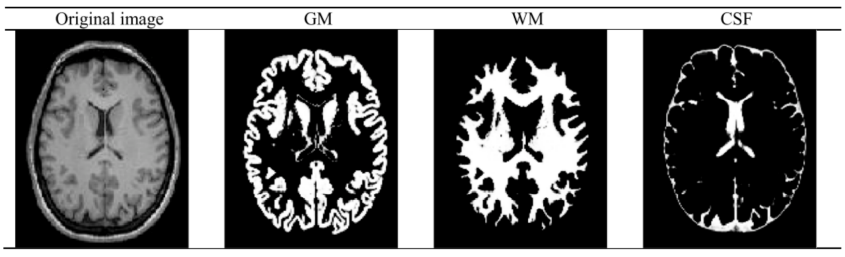

Figure 1.3: Segmentation of a brain MRI into gray matter (GM), white matter (WM), and CSF by Statistical Parametric Mapping (SPM) [2].

1.4 Classification of Brain Tumors

Brain tumors can be categorized by their biological behavior and histology. The World Health Organization (WHO) broadly classifies them as benign, premalignant, or malignant based on growth rate, invasiveness, and cellular atypia [10].

1.4.1 Benign Tumors

Benign tumors grow slowly and do not invade surrounding brain tissue. Histologically, their cells resemble normal counterparts and exhibit low mitotic activity. Common examples include meningiomas and pituitary adenomas, which often present with well-circumscribed margins and have favorable prognoses following surgical resection [10].

1.4.2 Premalignant Tumors

Premalignant lesions (WHO Grade I–II) display atypical cellular features and proliferative potential higher than benign lesions, yet lack overt invasive behavior. These tumors may progress to higher grades over time, and thus require close monitoring and, in some cases, adjuvant therapy.

1.4.3 Malignant Tumors

Malignant tumors (WHO Grade III–IV) are characterized by rapid growth, high mitotic index, and the ability to infiltrate adjacent neural structures. They often recur despite multimodal treatment (surgery, radiotherapy, chemotherapy) and carry poor overall survival [10].

1.5 Common Intracranial Tumor Types

The three most frequent primary brain tumors in adults are:

- **Meningioma.** Originating from the arachnoidal cap cells of the meninges, meningiomas are typically benign (WHO Grade I), slow-growing, and extra-axial. They often cause symptoms by mass effect rather than infiltration.
- **Pituitary Adenoma.** Arising in the anterior pituitary gland, these adenomas are usually benign but can lead to endocrine dysfunction and visual disturbances due to suprasellar

extension.

- **Glioma.** Gliomas arise from glial cells and represent the majority of malignant primary CNS tumors. They are graded by WHO as:
  - *Low-Grade Glioma (LGG, Grades I–II).* Slow-growing, with diffuse infiltration but relatively favorable prognosis.
  - *High-Grade Glioma (HGG, Grades III–IV).* Aggressive, with high proliferative index and poor survival; includes anaplastic astrocytoma (Grade III) and glioblastoma multiforme (Grade IV) [11].

Accurate grading of gliomas (LGG vs. HGG) is critical for treatment planning and prognosis, and motivates the need for precise segmentation and classification pipelines.

1.6 Signs and Symptoms Associated with Brain Tumors

Symptoms depend on tumor location, patient age, and growth rate, and include focal deficits (motor, seizure, visual, speech) and generalized signs (headache, nausea, dizziness, sleep disturbances) [12].

1.7 Diagnosis of Brain Tumors

The diagnosis of brain tumors is a complex process that requires a combination of clinical evaluation, imaging studies, and sometimes invasive procedures. The following sections outline the key components of this diagnostic process.

1.7.1 Physical Examination

One of the basics of this examination is that the doctor diagnoses the condition of the patient who is under suspicion of a brain tumor, where the doctor studies his condition by interrogating the patient to verify whether there are clinical signs that in turn lead the doctor to do a clinical examination that focuses on functions in which the brain intervenes, such as memory, emotions, understanding the language, feel of touch. By testing these functions, the peripheral symptoms can be detected, and therefore the affected area of the brain.

1.7.2 Complementary Examination

In most cases, the patient's condition requires the doctor to perform various tests, including a lumbar puncture. This is a test in which a sample of the spinal brain fluid is taken by sticking a needle into the lower stem of the spine, with the patient lying on the left side, a needle inserted into the L3 to L4 or L4 to L5. Afterwards, the sample is analyzed to find any cancer cells present for the tumor.

1.7.3 Brain Biopsy

Biopsy is a risky process that can cause bleeding while the surgeon is operating under the patient's total anesthesia, as well as a potential transmission of an infection, whether blood infection or other infection. The goal of this process is to search for cancer and determine its nature by surgically removing a sample of tissues taken from the tumor for closer examination to ascertain the nature of the tissues that are unknown.

1.7.4 Medical Imaging

This examination is based on imaging techniques such as MRI and computed tomography (CT) scanner or CT scan. MRI was adopted for its unique feature of having detailed, and also it is good technique for knowing the brain tumor in human body, where in the following we will present the general front and characteristics of it [13].

1.8 Megnatic Resonance Imaging (MRI)

Magnetic resonance imaging (MRI) uses a powerful magnetic field and radio waves to generate detailed and high-resolution images of organs and tissues inside the human body, as depicted in Figure 3.1. This non-invasive imaging method offers significant advantages in visualizing intricate details of the brain, spinal cord, joints, and soft tissues. MRI plays a vital role in diagnosing and evaluating a wide range of medical conditions, such as tumors, neurological disorders, and musculoskeletal injuries. Its ability to produce precise and detailed images aids healthcare professionals in accurately identifying and assessing these conditions, enabling effective treatment planning and optimal patient care [14].

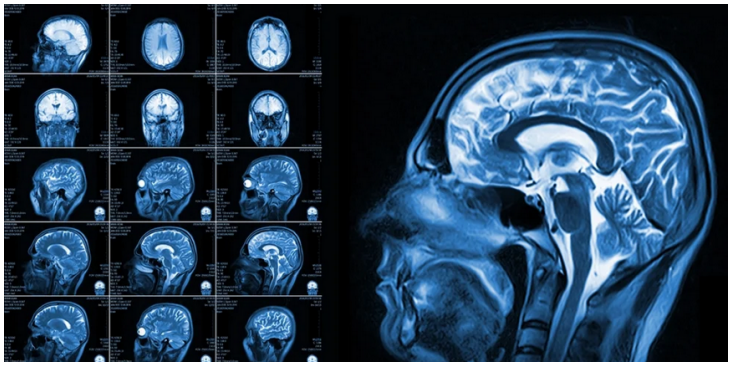

Figure 1.4: Magnetic Resonance Imaging (MRI).

1.9 Medical Imaging in Brain Tumor Diagnosis

Magnetic Resonance Imaging (MRI) has emerged as the gold standard for brain tumor diagnosis due to its superior soft tissue contrast, high spatial resolution, and non-invasive nature [15]. Unlike other imaging modalities such as CT scans, MRI provides detailed structural information without exposing patients to ionizing radiation, making it particularly valuable for serial monitoring and treatment planning [16].

The multimodal nature of MRI is especially useful in brain tumor assessment, with each sequence highlighting different aspects of the tumor [17]:

- **T1-weighted (T1)**: Provides excellent anatomical detail and clearly delineates boundaries between gray and white matter. Tumors typically appear hypointense (darker) compared to surrounding tissue.

Figure 1.5: Example of T1-weighted MRI sequence.

- **T1 with contrast enhancement (T1ce)**: After gadolinium administration, areas with disrupted blood-brain barrier (characteristic of high-grade tumors) enhance, appearing hyperintense and revealing the active tumor core.

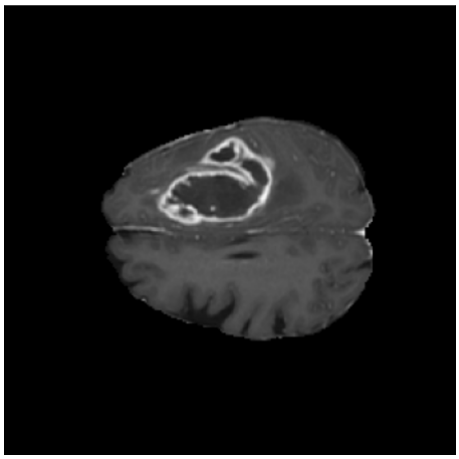

Figure 1.6: Example of T1-weighted contrast-enhanced MRI sequence.

- **T2-weighted (T2)**: Highlights areas with increased water content, making it valuable for identifying edema and infiltrative tumor components. Tumors and surrounding edema appear hyperintense.

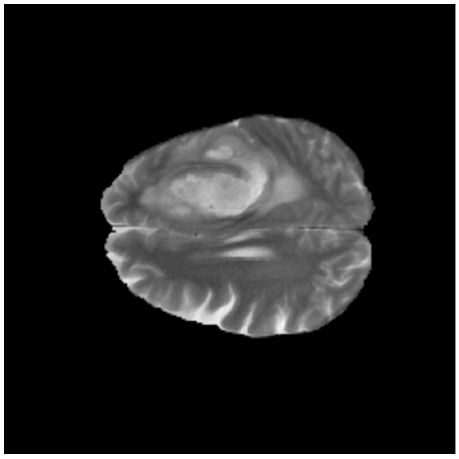

Figure 1.7: Example of T2-weighted MRI sequence.

- **Fluid-Attenuated Inversion Recovery (FLAIR)**: Suppresses cerebrospinal fluid signals, enhancing the visibility of periventricular lesions and edema associated with tumors.

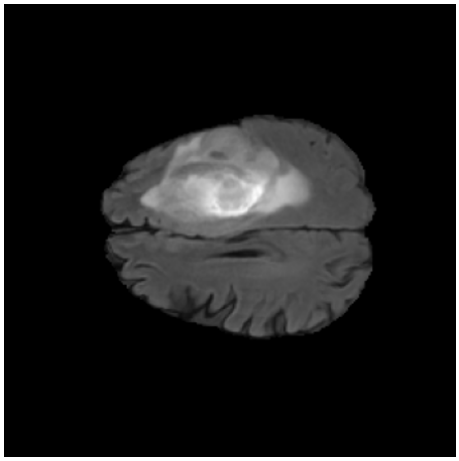

Figure 1.8: Example of FLAIR MRI sequence.

Traditionally, neuroradiologists diagnose brain tumors by visually inspecting these multiple MRI sequences, mentally integrating information across modalities to determine tumor boundaries, assess grade, and identify critical structures [18]. This process is inherently subjective, time-consuming, and susceptible to inter-observer variability, with studies reporting considerable disagreement even among experienced radiologists These limitations have driven significant interest in developing computational approaches for automated and semi-automated tumor analysis.

1.10 Conclusion

This chapter introduced the fundamental concepts of brain anatomy, tumor classification, and magnetic resonance imaging (MRI) modalities. We discussed the importance of accurate segmentation and classification of brain tumors and the traditional approach of manual diagnosis by radiologists. We also outlined the limitations and challenges of this approach, highlighting the need for computational methods to improve the accuracy and efficiency of brain tumor diagnosis.

Chapter 2

Deep Learning and Machine Learning

2.1 Introduction

Artificial intelligence (AI) has become indispensable in medical imaging, offering tools that can assist—and in some cases outperform—radiologists in detecting and characterizing pathologies. In the context of brain tumors, AI-driven methods enable rapid and accurate identification of tumor boundaries and grading, directly impacting treatment planning and patient outcomes.

In this chapter,

2.2 What is Artificial Intelligence?

Artificial Intelligence (AI) is a multidisciplinary field focused on developing machines and computer programs capable of performing tasks that typically require human intelligence, such as visual perception, reasoning, decision making, and language understanding. According to [19], AI is defined as:

> "the science and engineering of creating intelligent machines, particularly intelligent computer programs that can perform tasks requiring human intelligence, such as visual perception, decision making, and language translation."

In other words, AI includes both the study of human cognition—how people perceive,

learn, reason, and decide—and the development of algorithms and systems that can perform tasks requiring "intelligence," such as visual recognition or decision making. While some AI techniques draw inspiration from biological processes (e.g. neural networks), the field also embraces purely mathematical and statistical methods.

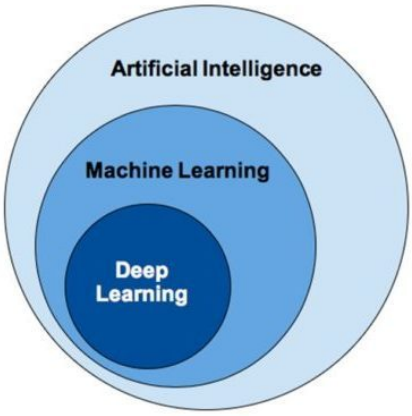

Figure 2.1: Differences between AI, machine learning, and deep learning. [3]

2.3 Machine Learning

Machine learning (ML) has emerged as a crucial area of study for organizations aiming to harness data resources and gain deeper insights into their operations. Unlike traditional programming methods, where explicit instructions are coded, machine learning enables systems to learn directly from data. In the medical imaging field, ML techniques offer powerful ways to analyze complex MRI data, supporting more accurate and efficient diagnostic processes. However, machine learning is a complex process that involves using diverse algorithms to iteratively learn from data, refine data representations, and make predictions. By feeding training data into these algorithms, increasingly accurate models can be developed. These machine learning models represent the knowledge acquired by algorithms during the training phase [20].

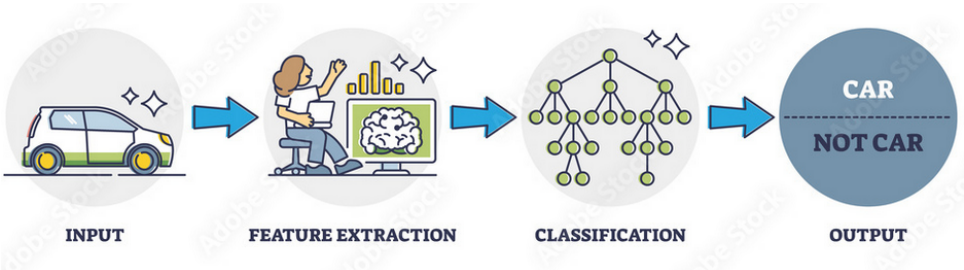

Figure 2.2: Machine learning process.

2.3.1 Machine Learning approachs

2.3.1.1 Supervised Learning

In supervised learning, the algorithm learns from labeled training data, where each data point is associated with a corresponding label or target value as depicted in Figure 2.3. Examples of supervised learning algorithms include linear regression , decision trees , random forests , support vector machines , and neural networks.

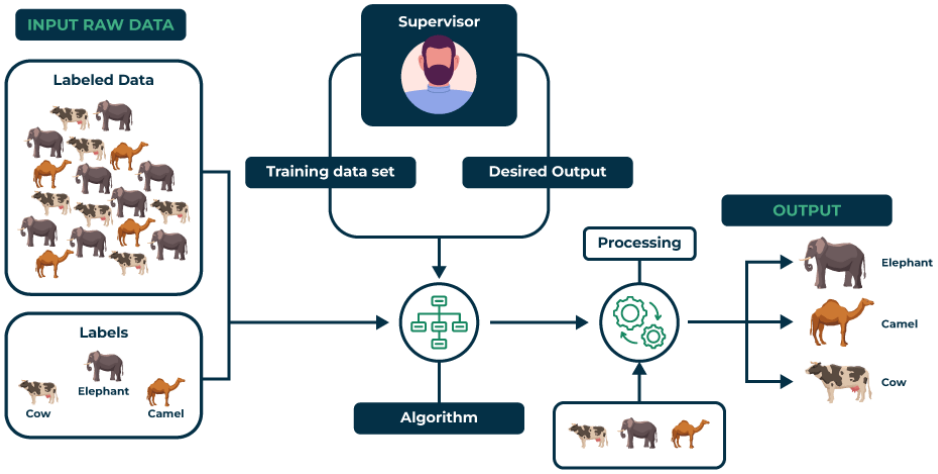

Figure 2.3: Supervised learning process.

2.3.1.2 Unsupervised Learning

Unsupervised learning deals with unlabeled data, where the algorithm learns to find patterns or structure in the data without any specific guidance. Such as k-means and hierarchical clustering, and dimensionality reduction techniques, such as principal component analysis and t-distributed stochastic neighbor embedding, Figure 2.4

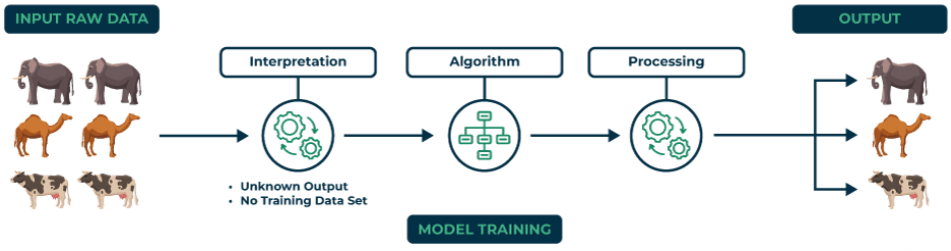

Figure 2.4: Unsupervised learning process.

2.3.1.3 Reinforcement Learning

Reinforcement learning is a type of machine learning where an agent learns to make decisions by interacting with an environment. The agent receives feedback in the form of rewards or penalties based on its actions, allowing it to learn optimal strategies over time. This approach is often used in robotics, game playing, and autonomous systems. Figure 2.5 illustrates the reinforcement learning process.

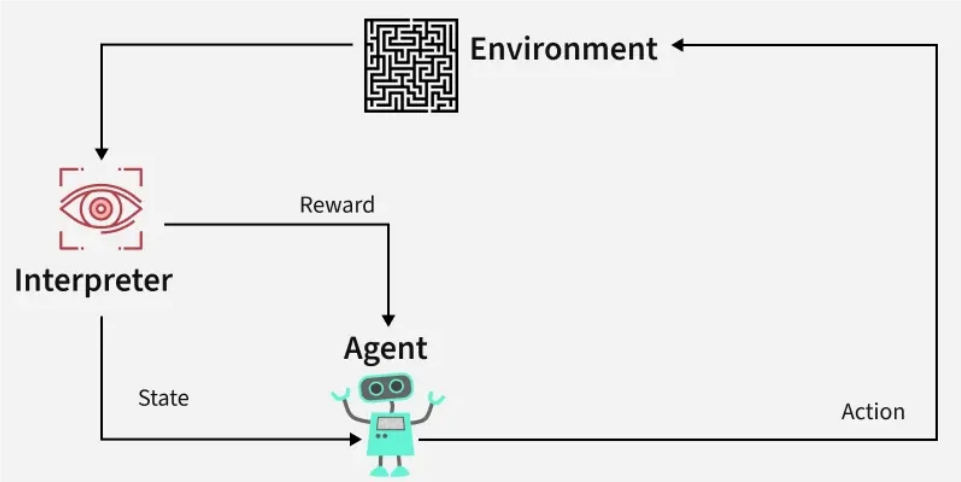

Figure 2.5: Reinforcement learning process.

2.3.2 Support Vector Machines (SVM)

Support Vector Machines (SVMs) are supervised machine learning models widely used for classification and regression tasks. The core idea of SVM is to find an optimal hyperplane that separates data points of different classes with the maximum possible margin, which enhances the model's ability to generalize to unseen data. SVMs can efficiently handle both linear and non-linear classification problems by employing the kernel trick, which implicitly maps input data into a higher-dimensional feature space where a linear separation becomes possible. The theoretical foundation of SVMs is based on the Structural Risk Minimization (SRM) principle, which aims to minimize an upper bound on the generalization error, offering advantages over traditional Empirical Risk Minimization approaches. Originally developed by Vapnik and colleagues in the 1990s, SVMs have become popular due to their strong empirical performance and robustness to overfitting, especially in high-dimensional spaces [21].

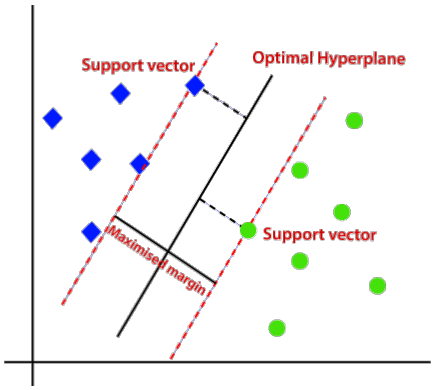

Figure 2.6: Support Vector Machine.

The fundamental formula defining the decision boundary of a Support Vector Machine (SVM) is a hyperplane expressed as:

$$\mathbf{w}^\top \mathbf{x} + b = 0 \tag{2.1}$$

where $\mathbf{w}$ is the weight vector normal to the hyperplane, $\mathbf{x}$ is the input feature vector, and b is the bias term.

For binary classification with labels $y_i \in \{+1, -1\}$, the SVM enforces the following constraints on each training point $(\mathbf{x}_i, y_i)$:

$$y_i\big(\mathbf{w}^\top \mathbf{x}_i + b\big) \;\geq\; 1, \quad \forall i. \tag{2.2}$$

The margin width (the distance between the closest points of each class to the hyperplane) is given by $\frac{2}{\|\mathbf{w}\|_2}$. Maximizing this margin is therefore equivalent to minimizing $\|\mathbf{w}\|_2$, leading to the following convex optimization problem:

$$\min_{\mathbf{w},b} \quad \frac{1}{2}\|\mathbf{w}\|_2^2, \tag{2.3}$$

$$\text{subject to} \quad y_i\big(\mathbf{w}^\top \mathbf{x}_i + b\big) \;\geq\; 1, \quad \forall i. \tag{2.4}$$

For non-linearly separable data, slack variables and kernel functions can be introduced, but the core formulation remains centered on maximizing the margin around this hyperplane.

2.4 Deep Learning

Deep learning has emerged as a powerful approach for modeling complex data through intricate architectures that incorporate non-linear transformations. Neural networks, including deep neural networks, serve as the fundamental components of deep learning. These techniques have achieved remarkable progress in various domains such as sound and image processing, enabling tasks like facial recognition, speech recognition, computer vision, language processing, and text classification. The potential applications of deep learning are vast and continue to expand.

Different types of neural network architectures, such as multilayer perceptrons, Convolutional Neural Networks (CNNs), and recurrent neural networks, cater to specific data types and tasks. These architectures are characterized by deep layers organized in a cascading manner. Successful implementation of deep learning requires well-designed stochastic optimization algorithms, appropriate initialization techniques, and thoughtful structure selection.

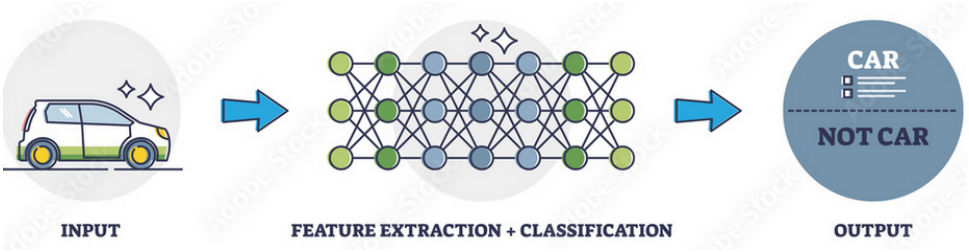

Figure 2.7: Deep learning process.

2.4.1 Convolutional Neural Networks (CNNs)

A convolutional neural network (CNN) is a type of neural network with a topology similar to a grid, inspired by the human brain. It is commonly used for image processing tasks, as well as natural language processing.

A CNN consists of two main parts. The input is an image, represented as a 2D matrix of pixels for grayscale images and a 3D matrix of pixels for color images (Red, Green, Blue).

The first part of a CNN is the convolutional layer, which acts as a feature extractor. The image is passed through a series of filters, or convolution kernels, to generate new images called feature maps. Some intermediate filters reduce the image resolution. Finally, the feature maps are concatenated to form a vector of features, known as the CNN code.

The output of the convolutional layer, the CNN code, is the input to the second part of the network. The main role of this part is to combine the features of the CNN code to classify the image. The output is a final layer with one neuron per category.

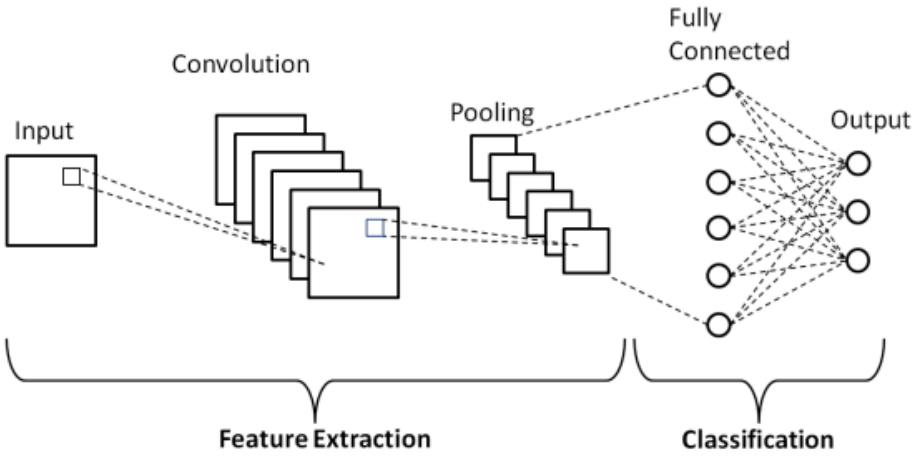

Figure 2.8: Convolutional Neural Network.

2.4.1.1 Convolutional Layer

The convolutional layer is the most important layer and usually the first layer in a CNN. It consists of three main elements involved in the convolution operation:

- **Input image** (f)
- **Feature detector (filter)** (h)
- **Feature map (output)** (G)

A convolution takes an image and a filter as input and applies the convolution operation to produce a new image, called the activation map or feature map.

The activation map values are calculated using the following formula:

$$G[m,n] = (f * h)[m,n] \tag{2.5}$$

where

- f is the input image,
- h is the convolution filter,

- m, n are the spatial indices over which the convolution is computed.

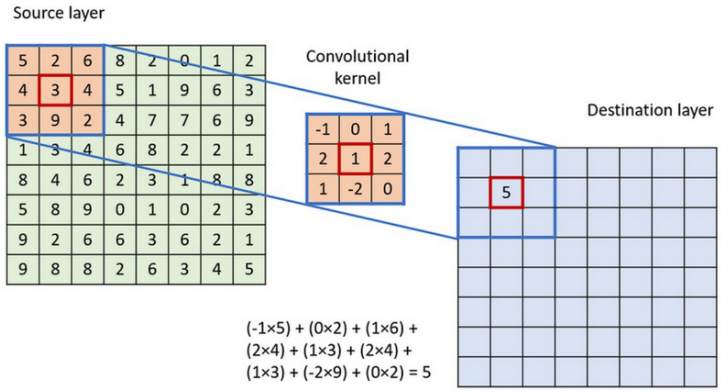

Figure 2.9: Convolution Layer.

2.4.1.2 Correction Layer (ReLU)

The Correction Layer, typically implemented using the Rectified Linear Unit (ReLU), is an activation function applied after each convolution operation to enhance processing efficiency. It replaces all negative pixel values with zero, introducing non-linearity into the network while maintaining computational simplicity. The ReLU function is defined as:

$$f(x) = \max(0, x) \tag{2.6}$$

Several other activation functions exist, such as the sigmoid function, the hyperbolic tangent function (tanh), and the hyperbolic saturating tangent function. However, ReLU is often preferred in deep learning models because it enables faster convergence and better performance compared to these alternatives.

2.4.1.3 Pooling Layers

Pooling layers are utilized to reduce the spatial dimensions of feature maps while preserving the most important information and features. This helps decrease computational complexity and mitigate overfitting. There are several types of pooling operations:

- **Max Pooling**: It selects the maximum value from each patch of the feature map. Typically, a 2×2 patch is used. Max pooling is the most commonly used pooling method.
- **Min Pooling**: The inverse of max pooling; it selects the minimum value from each patch

of the feature map.

- **Average Pooling**: It computes the average of all the values within each patch of the feature map by summing the values and dividing by the number of elements.
- **Sum Pooling**: It computes the sum of all elements within each patch of the feature map.
- **Flattening**: After the pooling operations, the resulting feature maps are flattened into a single one-dimensional vector to prepare for fully connected (dense) layers.

2.4.1.4 Fully Connected Layer

after the convolution and pooling layers, the high-level reasoning in the neural network is done in fully connected layers. The output of flattening is the input of FC layers which are the same as artificial neural networks and carry out the same mathematical operations. The last fully-connected layer uses an activation function such as sigmoid or softmax to get probabilities of the outputs.

2.4.2 U-Net Architecture

U-Net is a convolutional neural network architecture specifically designed for biomedical image segmentation. Introduced by Ronneberger et al. in 2015, U-Net features a symmetric encoder-decoder structure: the contracting path (encoder) captures image context through successive convolution and pooling operations, while the expansive path (decoder) enables precise localization via upsampling and concatenation with high-resolution features from the encoder. This architecture allows U-Net to achieve accurate segmentation even with limited annotated data by leveraging extensive data augmentation. U-Net has demonstrated superior performance in various biomedical segmentation challenges, notably outperforming previous methods in tasks such as neuronal structure segmentation in electron microscopy images and cell tracking in light microscopy [22].

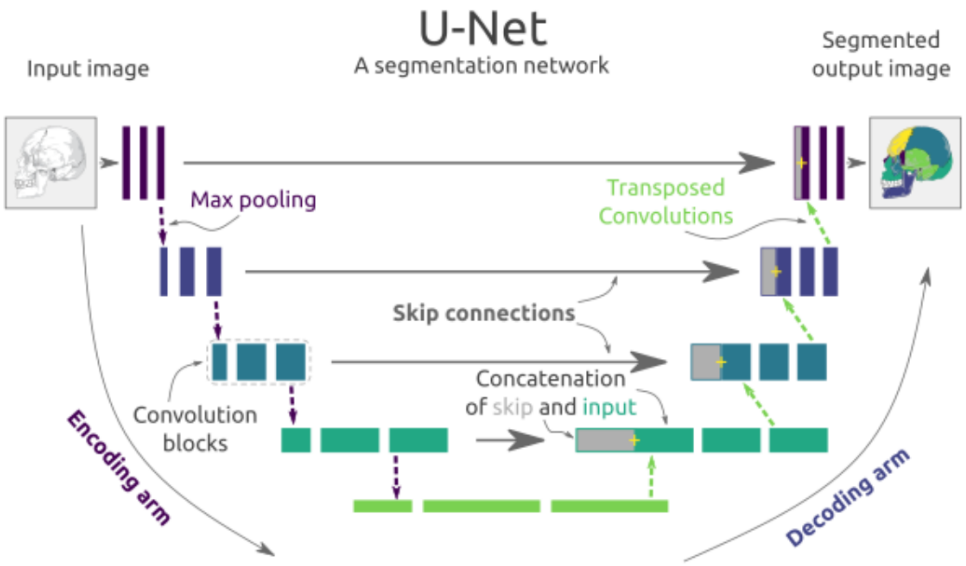

Figure 2.10: U-Net Architecture.

2.4.2.1 Key Components of a U-Net Architecture

- **Contracting Path (Encoder):**

  This path is responsible for extracting contextual features from the input image. It consists of repeated blocks of two 3×3 convolutional layers (with ReLU activation), followed by a 2×2 max pooling operation for downsampling. With each downsampling step, the number of feature channels is doubled, allowing the network to capture increasingly abstract representations of the input.

- **Bottleneck:**

  Located at the deepest part of the network, the bottleneck consists of convolutional layers without pooling. It serves as the bridge between the encoder and decoder, capturing the most condensed and abstract features of the input.

- **Expansive Path (Decoder):**

  This path reconstructs the spatial resolution of the feature maps and enables precise localization. Each step in the decoder involves upsampling the feature map (often via transposed convolution or up-convolution), concatenating it with the corresponding feature map from the encoder (skip connection), and then applying two 3×3 convolutions (with ReLU activation). The number of feature channels is halved at each upsampling step.

- **Skip Connections:**

  At each level, feature maps from the encoder are concatenated with the upsampled feature maps in the decoder. These skip connections help retain high-resolution spatial information that might otherwise be lost during downsampling, improving the accuracy of segmentation boundaries.

- **Final Output Layer:**

  The last layer is typically a 1×1 convolution that maps each feature vector to the desired number of output classes, producing a pixel-wise classification map for segmentation tasks.

This U-shaped design enables U-Net to effectively combine global context with fine-grained localization, making it highly effective for precise image segmentation tasks.

2.5 Conclusion

In this chapter, we established the theoretical foundation necessary for our study on brain tumor analysis using artificial intelligence techniques. We first explored the fundamental concepts of artificial intelligence, machine learning, and deep learning, emphasizing their significance in the medical imaging domain. We discussed the various machine learning approaches, highlighting the principles and applications of Support Vector Machines (SVMs) for classification tasks. Furthermore, we introduced deep learning methodologies, focusing on Convolutional Neural Networks (CNNs) and their components, including convolutional, pooling, and fully connected layers. Finally, we presented the U-Net architecture, a specialized CNN model for biomedical image segmentation, which plays a crucial role in the segmentation phase of our proposed hybrid approach. This theoretical background sets the stage for the practical implementation and evaluation of our models in the following chapters.

Chapter 3

State of the art on Brain Tumor Detection methods

3.1 Introduction

This chapter reviews the significant literature connected to this study, which aims to establish a conceptual information system framework for medical imaging employing MRI brain tumor pictures. The review focuses on the use of accessible current electronic scanners, computer-based methodologies, and their application to enhance the MRI brain tumor tissue analysis with a comparable accuracy to manual analysis methodology.

3.2 Literature Review

In this section, we will discuss the existing literature on the application of machine learning and deep learning techniques in the field of brain tumor detection.

3.2.1 Medical Imagery

Medical imaging is a technique that allows us to visualize the internal structure of a human body in order to diagnose various medical conditions.

3.2.1.1 Existing available approaches to analyze tissues

The routine examination of tissues is required to investigate the manifestations of the disease. With the availability of the medical images now, it provides a great opportunity to visualize tissue samples in order to diagnose various medical conditions. In order to make this diagnosis, there are three possible ways to perform this examination in the laboratory, including:

1. Traditional microscopic analysis.
2. Capturing the images using electronic devices and Analysis.
3. Computer based approaches using digitized images.

3.2.1.2 Traditional microscopic analysis

In the histopathology laboratory, professionals analyze slides of biopsy specimens using a microscope for counting and identification of different kinds of tissues. says that normally sample tissues acquired from a biopsy is cut into small segments (often 5 – 20 microns), processed and put onto glass slides. In addition to that preservation and staining is a component of processing the tissue segment in the fabrication of histopathology slides. 34

Generally, pathology professionals then conduct out manual inspection of these slides using a microscope as a regular job at different magnification levels (e.g. 10x, 20x, 40x, 100x, 200, 400x) to make judgements. Typically, histopathology slides are more informative than other modalities.

With advancements in computer power and the development of digital scanners and image processing tools, digital histopathology image analysis enables specialists to augment to help analyze the pictures. This decreases the time and effort necessary for diagnosis by pathologists as well as reduces human error and subjectivity. There are numerous sorts of digital scanners accessible at today to study various types of tissue structures which include Ultrasound, CT, MRI, PET.

3.2.1.3 Capturing the images using electronic devices

From what we mentioned, ultrasound despite its wide fame in the field of medical imaging and its low risk to patients. However, it is limited from the side that it cannot treat small tissues, as it is only specialized for large tissues. Compared to ultrasound, the use of CT and MRI delivers better when considering cancer tissues especially brain tumors and among CT and MRI. Among CT and MRI, MRI provides greater soft tissue contrast than other techniques because it can present in detail and can distinguish tissues in the brain. MRI are considered safe for patients to avoid harmful effects because they do not use ionizing radiation during the examination, and provide more detail than CT images.

3.2.1.4 Computer-Aided methods using digitized images obtained from biopsy specimen slides

Manual microscopic examination is time intensive, prone to mistakes and produces uneven results among specialists. Most utilized electronic scanner like ultrasound can only detect big and mature follicles. Additionally, CT, MRI and UT need professionals' assistance. To solve the challenges connected with microscopic analysis and electronic scanners computer-based techniques would be a feasible solution since computerized image analysis minimizes time, effort, human mistakes and subjectivity for the diagnosis of diverse tissues by pathologists. There are several sorts of 35current computer-based methodologies accessible at present which largely considers cancer tissue analysis, blood vessel analysis and lymphatic channel analysis. While there are so many current ways accessible to date yet none of the present approaches are suited to evaluate MRI brain tumor tissues. This is owing to the fact that none of the available systems are totally automated which do not need any human interaction when assessing a fresh batch of photographs.

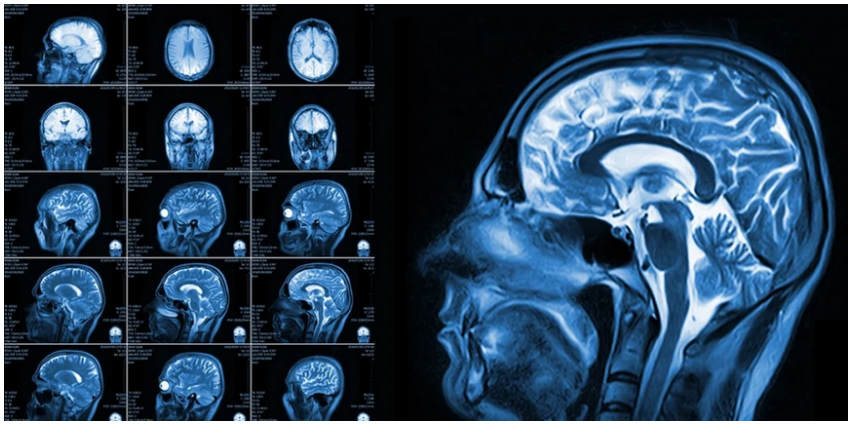

Figure 3.1: Example of brain MRI image. [4]

3.2.2 Image processing techniques

3.2.2.1 Image Pre-processing

The medical images processed contain a great deal of information as they are usually noisy due to unwanted pixels. it is always necessary to preprocess as a first step in most current image analysis techniques to analyze the image of the brain tumor where pre-processing aims to improve:

1. **Noise removal**: Removing impulse noise from images is one of the most important concerns in digital image processing, where noise must be removed in a way that preserves the important information of the image. A variety of techniques are used to eliminate and reduce noise in images, including a Gaussian filter, which is used to remove details and noise. It provides positive and enhanced results for noisy images.

2. **Enhance contrast**: It is defined as the manipulation and redistributing the image pixels in a linear or non-linear fashion to improve the separation of obscured structural variations in pixel intensity into a more visually differentiable structural distribution [23]. However, there is no universal theory for enhance contrast approach [24]. Digitized images acquired from MRI are typically grayscale images. It is hard to deal with the intensity of a grayscale image straightway [24]. The processing of contrast enhancement histograms is one of the most widely used approaches. The processing of histogram includes equalization (An approach that extends the intensity range and improves image contrast.) and normalization (An approach for modifying the series of pixel intensity values according to relative frequencies).

3.2.2.2 Segmentation

Segmentation is the most important part in image processing. Fence off an entire image into several parts which is something more meaningful and easier for further process. These several parts that are rejoined will cover the entire image. Segmentation may also depend on various features that are contained in the image. It may be either color or texture. Before denoising an image, it is segmented to recover the original image. The main motto of segmentation is to reduce the information for easy analysis. Segmentation is also useful in Image Analysis and Image Compression [25].

3.2.2.3 classification

Although there are many techniques used to identify and classify each depending on the characteristics they target for detection, for images of MRI brain tumor, there are three basic characteristics (shape, size, and color) required for tumor detection. In most cases, the svm algorithm is used, but more recently, the Convolutional Neural Network approach is also widely used in medical image processing.

3.2.2.4 Detection

Image detection is a technique that analyzes the picture and finds items inside it, medical image detection refers to the process of recognizing medical-related objects that are included within an image. This assists in establishing the precise placement of multiple tissues as well as the direction of those tissues.

3.3 Related Work

In this section, we review key approaches to brain tumor segmentation and classification that motivated our work. We focus on five representative studies, highlighting their main techniques and results, and then summarize them in Table 3.1.

3.3.1 Brain Tumor Segmentation and Grading of Lower-Grade Glioma

Naser *et al.* [26] used a U-Net–based CNN with transfer learning from VGG16 to segment tumors in 110 T1-FLAIR cases of low-grade glioma (LGG). They then classified LGG into

grade II vs III, achieving 89 % accuracy on slice-level MRI and 95 % at the patient level. In contrast, our work employs transfer learning to distinguish among three tumor types rather than grades, and omits mask-based classification in favor of position and texture cues.

3.3.2 Wavelet Statistical Texture + RNN

Begum *et al.* [27] combined optimal wavelet statistical features with an RNN classifier. Their pipeline includes Gaussian filtering for noise removal, OGSA-based feature selection, RNN classification, and tumor ROI segmentation via a modified region growing algorithm (MRG). They reported 95 % accuracy. Our approach instead uses skull stripping with morphological dilation/erosion (and GrabCut verification) to eliminate noise without explicit filtering.

3.3.3 Hybrid CNN + NADE

Hashem *et al.* [28] trained two parallel CNNs whose feature outputs are combined via a Neural Autoregressive Distribution Estimator (NADE). This joint distribution aids in tumor shape identification. Using cross-entropy loss on 3 064 T1-weighted images (6-fold CV), they achieved 95 % accuracy. We similarly verify segmentation masks with GrabCut, but replace NADE's distribution estimation with model-derived morphological consistency checks.

3.3.4 Hierarchical Transfer Learning with AlexNet & GoogleNet

The framework in [29] applies skull stripping and then uses AlexNet to classify tumors into benign vs malignant, followed by GoogleNet to further distinguish malignant into glioma vs meningioma. With data augmentation (flips, rotations), they report:

- Benign vs Malignant: precision 93.75 %, recall 100 %, F1 96 %.
- Glioma vs Meningioma: precision 95 %, recall 100 %, F1 97.43 %, accuracy 97.50 %.

Our demo uses a single-stage classifier for three tumor types, with GrabCut–verified skull stripping to preserve T1-FLAIR properties.

3.3.5 VGG Block-wise Fine-Tuning

Lee *et al.* [30] employ VGG19 with a block-wise fine-tuning strategy, dividing the network into six blocks and progressively unfreezing from the last block. Evaluated on the same 3 064 T1-weighted set (5-fold CV), they reach 94.42 % accuracy. We adopt transfer learning as well but use discriminative slanted triangular learning rates rather than linear schedules for fine-tuning.

Table 3.1: Summary of prior methods in brain tumor segmentation and classification

Study	**Approach**	**Dataset**	**Key Results**
Naser *et al.* [26]	U-Net + VGG16 transfer learning	110 LGG (T1-FLAIR)	MRI accuracy: 89%, patient accuracy: 95%
Begum *et al.* [27]	OGSA wavelet + RNN + MRG segmentation	BraTS2020 (?)	95% accuracy
Hashem *et al.* [28]	Hybrid CNNs + NADE	3,064 T1-weighted images	95% (6-fold CV)
Framework [29]	AlexNet → GoogleNet hierarchy	BraTS2020 (?)	Benign vs Mal: F1 96%; Glioma vs Men: F1 97.43%, acc 97.50%
Lee *et al.* [30]	VGG19 block-wise fine-tuning	3,064 T1-weighted images	94.42% (5-fold CV)

3.4 Conclusion

In this chapter, we reviewed key approaches to brain tumor segmentation and classification, highlighting the most utilized machine learning and deep learning models for this purpose. We examined studies that informed our work, focusing on their methodologies and results.

Chapter 4

Methodology and Contribution

4.1 Introduction

In this chapter, we present the core contributions of our work on automated brain tumor detection in magnetic resonance (MR) images. Building upon the BraTS benchmark dataset [16], our pipeline integrates a deep learning–based segmentation module with a classical machine learning classifier and culminates in a user-friendly demo application. The main objectives of this chapter are:

- To describe a tailored U-Net–based segmentation pipeline for delineating tumor subregions in MRI slices.
- To detail a feature-extraction and SVM classification scheme that distinguishes high-grade from low-grade gliomas using volumetric, intensity, texture, and shape descriptors.
- To demonstrate the integration of these modules within an end-to-end application for streamlined inference on new patient data.

The remainder of this chapter is organized as follows. In Section 4.3, we introduce the dataset and preprocessing steps. Section 4.4 details the U-Net segmentation module, including architecture and training protocol. Section 4.5 covers the feature engineering and SVM classification. Section 4.6 presents the design and functionality of our demo application. We conclude with a discussion of key findings and future directions.

4.2 Proposed Framework Overview

In this section, we look at our proposed fremework from a systematic perspective. The framework is designed to perform end-to-end brain tumor segmentation and classification. We will discuss the design of the final pipeline and the training workflow to achieve the desired results.

4.2.1 End-to-End Inference Pipeline

The purpose of our project is to have an end-to-end inference pipeline accepts a raw MR image as input, applies preprocessing steps, performs segmentation of the tumor region using the trained U-Net model, classifies the tumor grade via the SVM classifier, and finally outputs the original image overlaid with the segmentation mask along with the predicted grade.

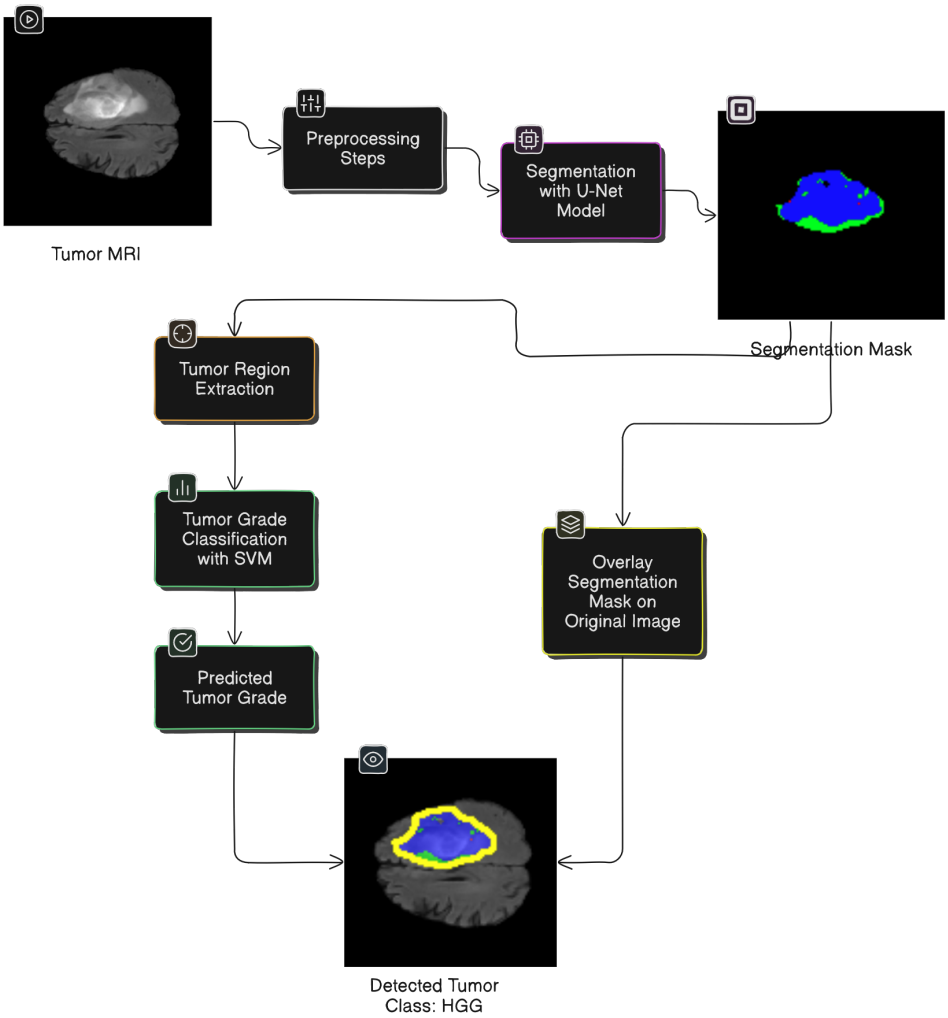

Figure 4.1: Overview of the end-to-end inference pipeline.

4.2.2 Model Training Workflow

The training workflow begins with the BraTS dataset. After preprocessing and augmentation, the data is split into training, validation, and test sets. We then train the U-Net segmentation model in parallel with feature extraction followed by SVM classifier training, yielding two standalone models for inference.

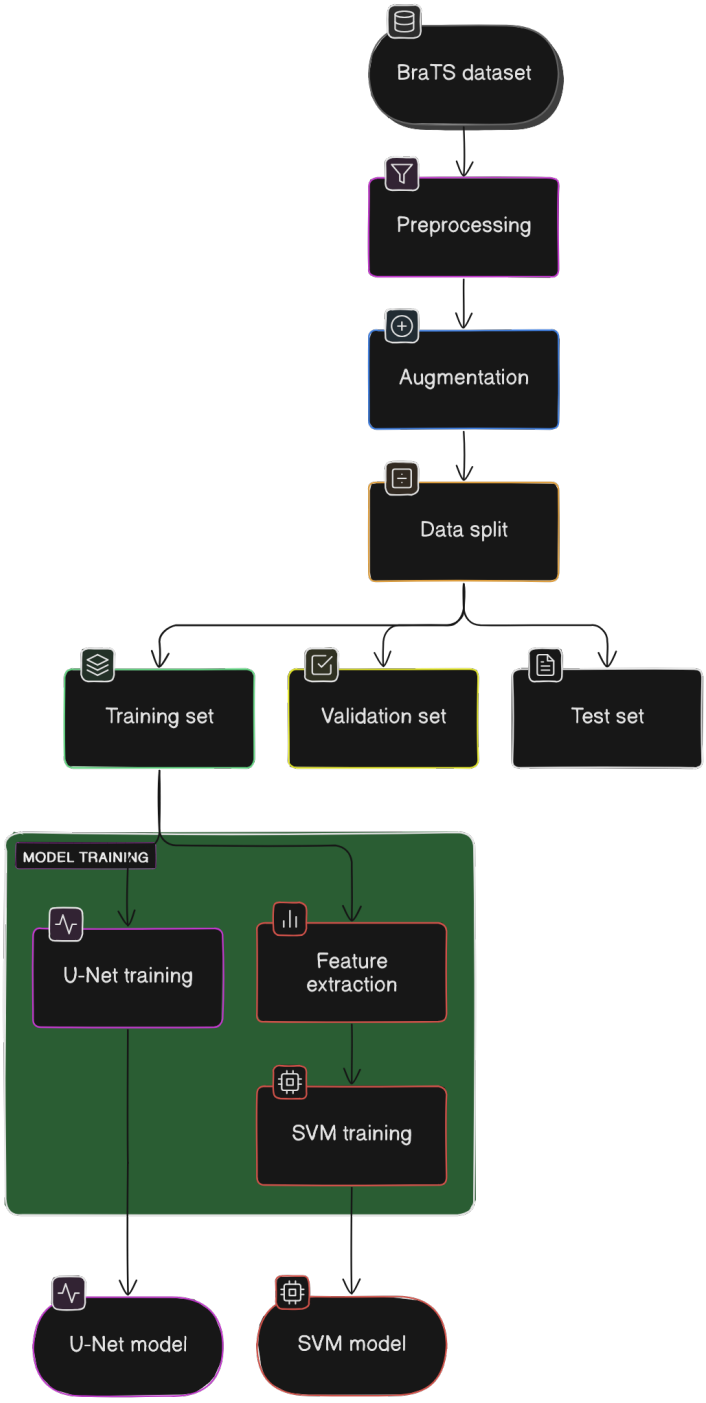

Figure 4.2: Overview of the training workflow.

4.3 Dataset and Preprocessing

In order to train our hybrid model we used the Brain Tumor Segmentation (BraTS) 2020 dataset, which is a collection of multimodal Magnetic Resonance Imaging (MRI) scans used for the segmentation of brain tumors.

4.3.1 BraTS Dataset Description

The dataset includes MRI scans from glioma patients, providing four different MRI modalities per patient:

1. **Native (T1)**
2. **Post-contrast T1-weighted (T1ce - contrast enhanced)**
3. **T2-weighted (T2)**
4. **T2-FLAIR (T2 - Fluid Attenuated Inversion Recovery)**
5. **Tumor Segmentation Mask**

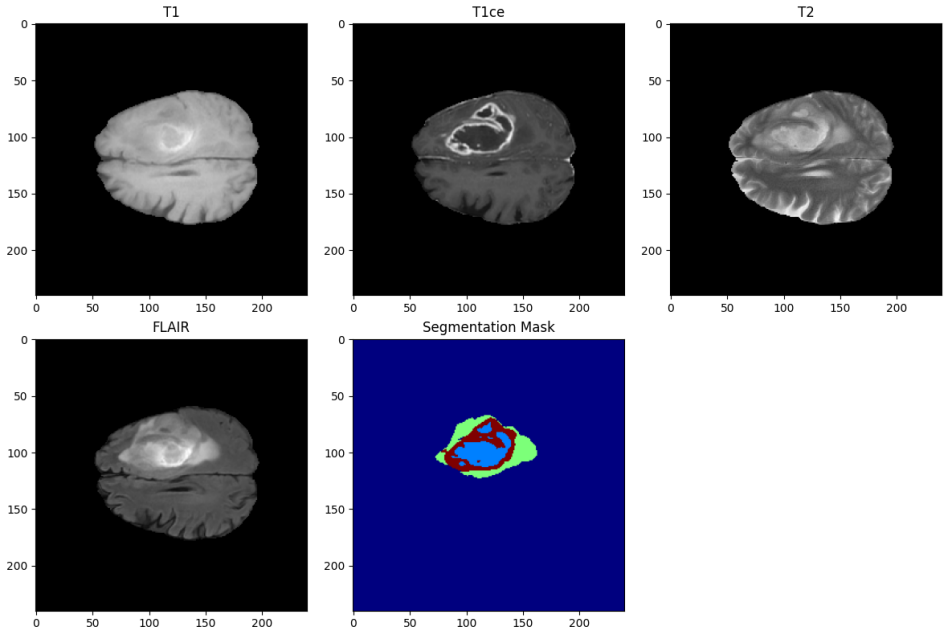

Figure 4.3: Brats modalities: T1, T1ce, T2, and T2-FLAIR.

These scans come with expert-annotated segmentation masks that delineate the tumor into various sub-regions, such as the necrotic and non-enhancing tumor core, the peritumoral edema,

and the enhancing tumor. Research has demonstrated that accurate segmentation is linked to improved prognostic assessments and treatment outcomes.

- **Class 0 (Not Tumor):** This class represents normal brain tissue or background, where no tumor tissue is present.
- **Class 1 (Non-Enhancing Tumor):** This class corresponds to the necrotic or non-enhancing core regions of the tumor. These areas typically lack contrast enhancement and may include dead or less active tumor tissue.
- **Class 2 (Edema):** This class identifies regions of peritumoral edema, which is the swelling around the tumor caused by fluid accumulation. Edema is important for understanding the extent of the tumor's impact on surrounding brain tissue.
- **Class 4 (Enhancing Tumor):** This class captures the actively enhancing parts of the tumor, visible after the administration of a contrast agent. These regions often indicate aggressive tumor tissue with increased blood flow and permeability.

To visually interpret these segmentations, we map the categorical labels to a custom colormap. In our example, we use four distinct colors to represent:

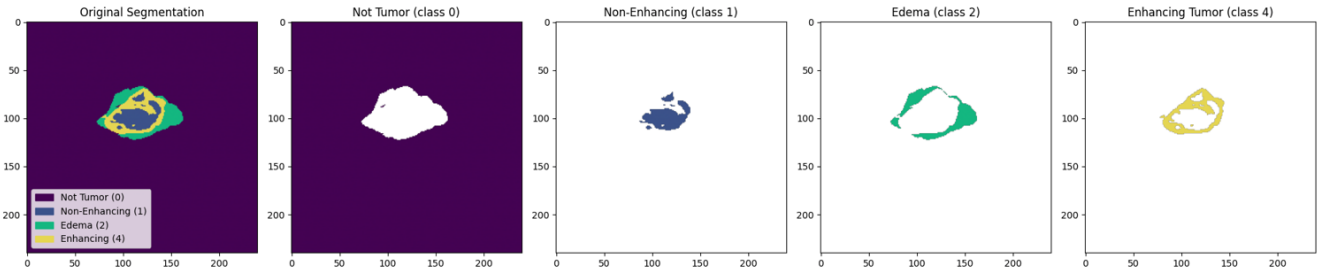

Figure 4.4: Segmentation of Tumor classes.

4.3.2 Dataset Splitting

To train and evaluate our model effectively, we need to partition our dataset into three subsets:

- **Training Set (70%):** Used to learn the model parameters.
- **Validation Set (approximately 20%):** Used for tuning hyperparameters and preventing overfitting.

- **Test Set (10%):** Used for assessing the final model's performance on unseen data.

This split can be done randomly or in a stratified manner (to preserve the class distribution), which is especially useful when dealing with imbalanced datasets. Properly splitting the dataset is crucial for building a robust model that generalizes well to new data.

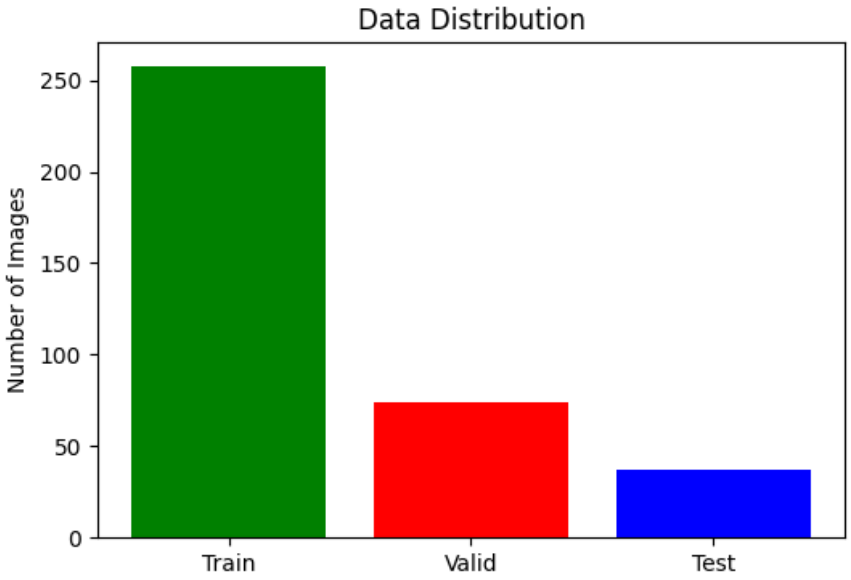

Figure 4.5: Distribution of the training, validation, and test sets.

4.3.3 Data Preprocessing

Before feeding MR volumes into our models, we apply a series of standardized preprocessing steps to ensure consistency and improve model robustness. Our pipeline operates on 2D axial slices extracted from 3D volumes, as follows:

1. **Slice Extraction.** For each patient volume, we select 100 consecutive axial slices starting at index 22. This avoids initial and final slices that contain little anatomical information.

2. **Resizing.**

   - *Image Slices:* Each extracted slice is resized to 128×128 pixels to match the U-Net input dimensions.

   - *Segmentation Masks:* Corresponding ground-truth masks are first resized to 240×240 (to preserve label fidelity) and later downsampled alongside images during one-hot

encoding.

3. **Intensity Normalization.** All pixel intensities in a slice are divided by the global maximum value of that volume, scaling inputs to the $[0, 1]$ range. This step harmonizes contrast across patients and modalities.

4. **Augmentation.** To increase effective training diversity, random geometric transformations are applied during batch generation:

   - Horizontal and vertical flips (each with 50% probability).
   - Rotations by multiples of 90° (randomly chosen among 0°, 90°, 180°, 270°).

These preprocessing routines standardize input dimensions, normalize intensity distributions, and inject variability—laying a solid foundation for both segmentation and classification tasks.

4.4 Segmentation Module

The segmentation module is responsible for delineating tumor subregions in MR slices. It consists of a U-Net–based convolutional network for mask prediction.

4.4.1 U-Net Architecture

Our U-Net follows the standard encoder–decoder pattern with skip connections:

- **Encoder:** Four downsampling blocks, each with two `Conv2D` layers (kernel size 3×3, `ReLU` activation) followed by `MaxPooling2D`.
- **Bottleneck:** Two `Conv2D` layers at the lowest resolution, with a dropout of 0.2 to reduce overfitting.
- **Decoder:** Four upsampling blocks, each using `UpSampling2D` + `Conv2D (2×2)` and concatenation with the corresponding encoder feature map.
- **Output:** A final `Conv2D` layer with a 1×1 kernel and `softmax` activation to produce a four-channel segmentation mask.

4.4.2 Evaluation Metrics for Segmentation

In segmentation tasks, *accuracy* measures the overall proportion of correctly classified pixels. However, in datasets like BraTS2020—where the background (non-tumor) pixels vastly outnumber tumor pixels—accuracy can be misleading. Therefore, we employ the following metrics for a more balanced evaluation:

- **Precision** (Positive Predictive Value) Measures the fraction of predicted tumor pixels that are truly tumor:

$$\text{Precision} = \frac{\text{TP}}{\text{TP}+\text{FP}}$$

  where

  - TP = number of true positive pixels,
  - FP = number of false positive pixels.

- **Sensitivity** (Recall or True Positive Rate) Measures the fraction of actual tumor pixels correctly identified:

$$\text{Sensitivity} = \frac{\text{TP}}{\text{TP}+\text{FN}}$$

  where

  - FN = number of false negative pixels.

- **Specificity** (True Negative Rate) Measures the fraction of non-tumor pixels correctly classified:

$$\text{Specificity} = \frac{\text{TN}}{\text{TN}+\text{FP}}$$

  where

  - TN = number of true negative pixels.

- **Intersection over Union (IoU)** Also known as the Jaccard index, IoU measures overlap between prediction and ground truth:

$$\text{IoU} = \frac{\text{TP}}{\text{TP}+\text{FP}+\text{FN}}.$$

  We report the *mean IoU* (mIoU) averaged over the four classes.

- **Dice Coefficient** (F1 Score) The Dice coefficient emphasizes overlap and is defined as:

$$\text{Dice} = \frac{2\,\text{TP}}{2\,\text{TP} + \text{FP} + \text{FN}}.$$

We compute both the *overall Dice* (averaged across classes) and *per-class Dice* for necrotic/core, edema, and enhancing tissue.

4.4.3 Segmentation Results

In this section, we present the results of our U-Net segmentation model on the BraTS2020 dataset. The model was trained for 50 epochs with a batch size of 16, we will discuss the end results of the training and validation process, including loss and accuracy metrics.

4.4.3.1 Accuracy

The model achieved an impressive pixel-level accuracy of 99.3%, indicating that the vast majority of pixels were correctly classified. This high accuracy is particularly important in medical imaging, where even small errors can have significant implications.

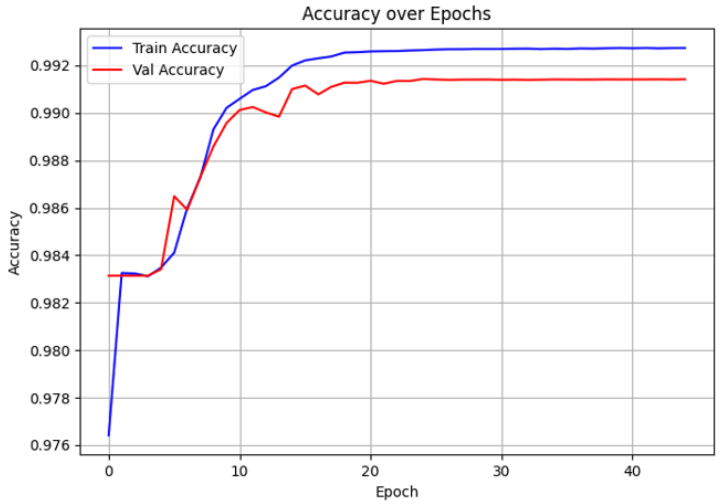

Figure 4.6: Segmentation accuracy over epochs.

4.4.3.2 Loss

The loss function used during training was the categorical cross-entropy loss, which measures the dissimilarity between the predicted and true distributions. The model converged to a low loss of 0.0231, indicating that the predictions were closely aligned with the ground truth.

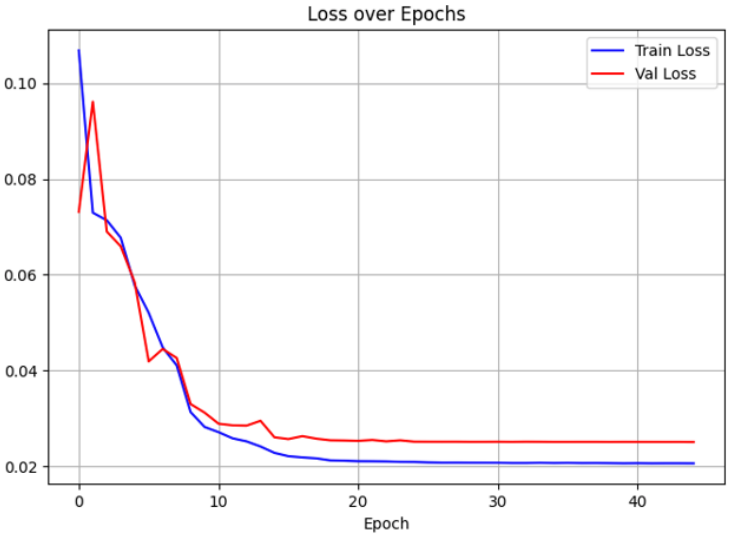

Figure 4.7: Segmentation loss over epochs.

4.4.3.3 Dice Coefficient

The Dice coefficient is a measure of overlap between the predicted and true segmentation masks. The overall Dice coefficient achieved was 58.98%, indicating a good level of agreement between the predicted and true tumor regions. The per-class Dice coefficients were also calculated, providing insights into the model's performance on different tumor subregions.

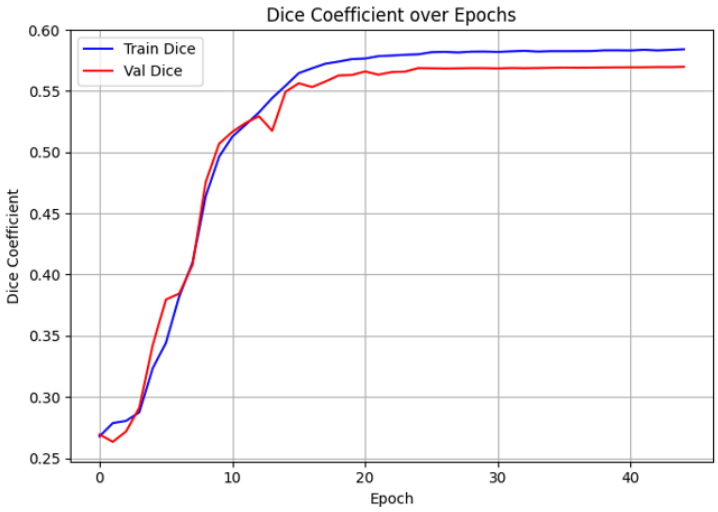

Figure 4.8: Segmentation Dice coefficient over epochs.

4.4.3.4 Mean IoU

The mean Intersection over Union (IoU) was calculated to assess the model's performance across all classes. The mean IoU achieved was 74.66%, indicating a good level of overlap be-

tween the predicted and true segmentation masks. This metric is particularly useful in medical imaging, where accurate delineation of tumor boundaries is crucial for treatment planning.

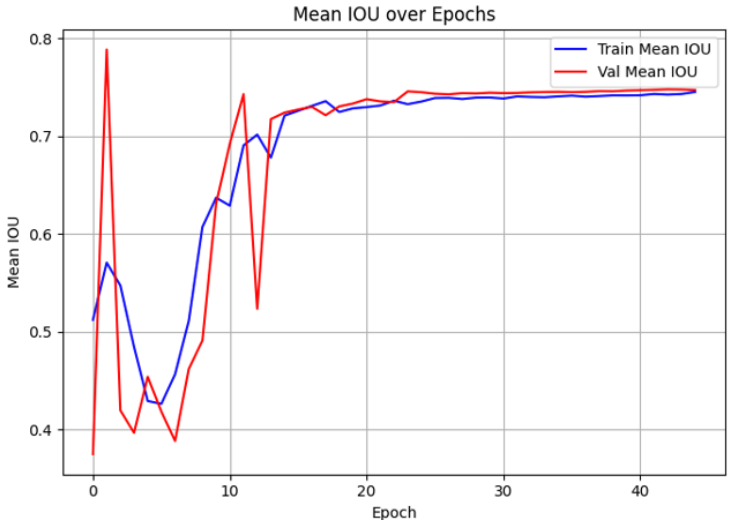

Figure 4.9: Segmentation mean IoU over epochs.

Table 4.1 summarizes the quantitative performance, and Figure 4.10 shows a representative qualitative result.

Table 4.1: Segmentation performance on the test set

Metric	**Value**
Loss	0.0231
Accuracy	99.30 %
Mean IoU	74.66 %
Dice Coefficient (overall)	58.98 %
Precision	99.37 %
Sensitivity	99.08 %
Specificity	99.79 %

Overall, the model converged to a low loss (0.0231) and achieved excellent pixel-level accuracy (99.3 %), demonstrating strong background discrimination (specificity = 99.8 %). The mean IoU of 74.7 % and overall Dice of 59.0 % indicate reliable overlap between prediction and ground truth also confirms that tumor regions are both accurately and comprehensively detected.

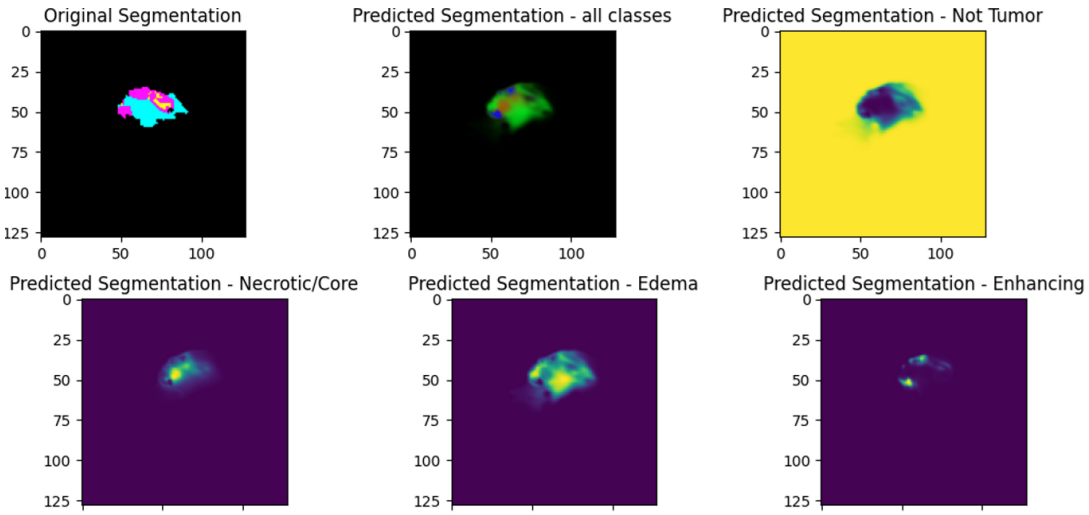

Figure 4.10: Example of segmentation results.

4.5 Classification Module

The classification module distinguishes high-grade gliomas (HGG) from low-grade gliomas (LGG) using handcrafted features extracted from the segmented tumor regions and a support vector machine (SVM) classifier.

4.5.1 Feature Extraction

From each segmented case, we compute the following feature categories:

- **Volume Features:** Volumes of necrotic/core (NCR), edema (ED), enhancing tumor (ET), tumor core (TC), and whole tumor (WT), plus their ratios (e.g., TC/WT, ET/TC).
- **Intensity Statistics:** Mean, standard deviation, minimum, maximum, median, 10th/90th percentiles, and range of voxel intensities for each modality (FLAIR, T1, T1CE, T2) within each tumor component.
- **Texture Features:** Histogram of oriented gradients (HOG)–based descriptors computed on each component.
- **Shape Features:** Extents along each axis, elongation, flatness, and sphericity of the whole tumor mask.
- **Heterogeneity Features:** Contrast between core and edema, and between enhancing and necrotic regions for each modality.

4.5.2 Feature Selection

- Fit a Random Forest classifier on the training split to compute feature importances.
- Select the top 30 most important features for downstream classification.

4.5.3 SVM Model Training

- **Data Split:** 80% training, 20% test (stratified by grade).
- **Scaling:** Standardize features to zero mean and unit variance.
- **Hyperparameter Search:** Grid search over $\{C \in [0.1, 1, 10, 100]\}$, $\gamma \in \{\text{scale}, \text{auto}, 0.01, 0.1\}$, and $\{\text{rbf}, \text{linear}, \text{poly}\}$ kernels, using 5-fold CV.
- **Final Model:** Best-estimator SVM retrained on full training set.

4.5.4 Evaluation Metrics for Classification

We assess performance on the held-out test set using:

- **Accuracy:** Fraction of correctly classified patients.

$$\text{Accuracy} = \frac{\text{TP} + \text{TN}}{\text{TP} + \text{TN} + \text{FP} + \text{FN}}$$

- **Precision, Recall, F1-Score:** Computed per class and averaged.

$$\text{Precision} = \frac{\text{TP}}{\text{TP} + \text{FP}}, \qquad \text{Recall} = \frac{\text{TP}}{\text{TP} + \text{FN}}, \qquad \text{F1} = \frac{2 \cdot \text{TP}}{2 \cdot \text{TP} + \text{FP} + \text{FN}}$$

- **Confusion Matrix:** Counts of true vs. predicted labels.
- **ROC AUC:** Area under the receiver operating characteristic curve.

$$\text{AUC} = \frac{1}{2} \sum_{i=1}^{n} (\text{TPR}_i + \text{TPR}_{i-1}) \cdot (\text{FPR}_i - \text{FPR}_{i-1})$$

where n is the number of thresholds and TPR_i and FPR_i are the true positive and false positive rates at the ith threshold.

4.5.5 Classification Results

The SVM classifier was optimized via grid search, yielding the following best hyperparameters:

- $C = 1$, $\gamma =$ scale, Kernel = `linear`

On the held-out test set (74 patients), the model achieved an overall accuracy of 93.24 %.

Table 4.2: Classification report

Class	Precision	Recall	F1-Score	Support
LGG (0)	86 %	80 %	83 %	15
HGG (1)	95 %	97 %	96 %	59
Accuracy		93.24 %		
Macro avg	90 %	88 %	89 %	74
Weighted avg	93 %	93 %	93 %	74

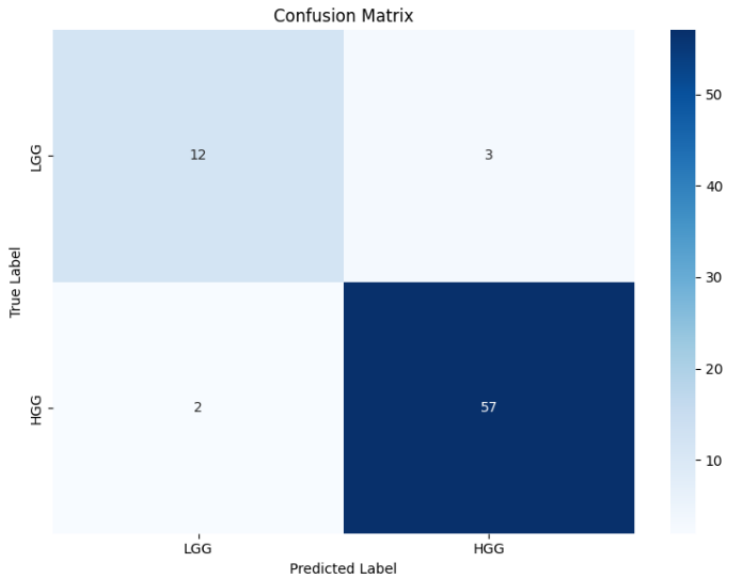

Figure 4.11: Confusion matrix for the SVM classifier.

Example Inference On a new patient (ID 083), the pipeline predicted:

- **Prediction:** HGG
- **Probability of HGG:** 93.60 %
- **Actual Grade:** HGG (correct)

4.6 Application Demo

To illustrate end-user interaction, we developed a lightweight demo application that integrates our trained U-Net and SVM models into a single GUI. The application consists of two main pages:

4.6.1 Upload Page

Presents an HTML form where the user can select and upload a brain tumor image (2D slice). Upon submission, the form sends a POST request to the `/results` route.

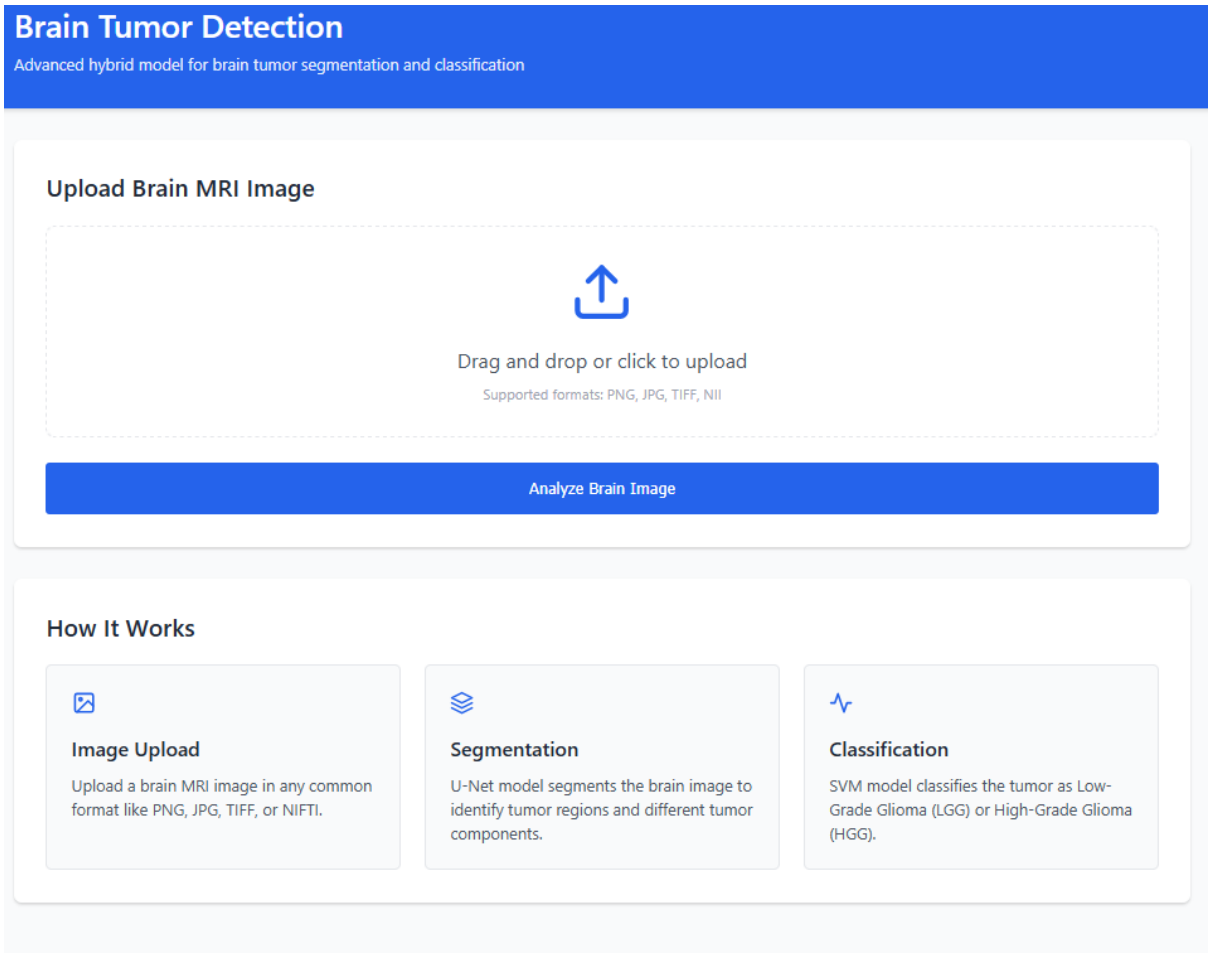

Figure 4.12: Upload page of the application demo.

4.6.2 Results Page

Receives the uploaded image, runs the preprocessing, segmentation (U-Net), feature extraction, and classification (SVM) pipeline, and then renders:

- The original input image.
- The segmentation mask overlaid on the input.
- The predicted tumor grade (LGG/HGG) with its confidence score.

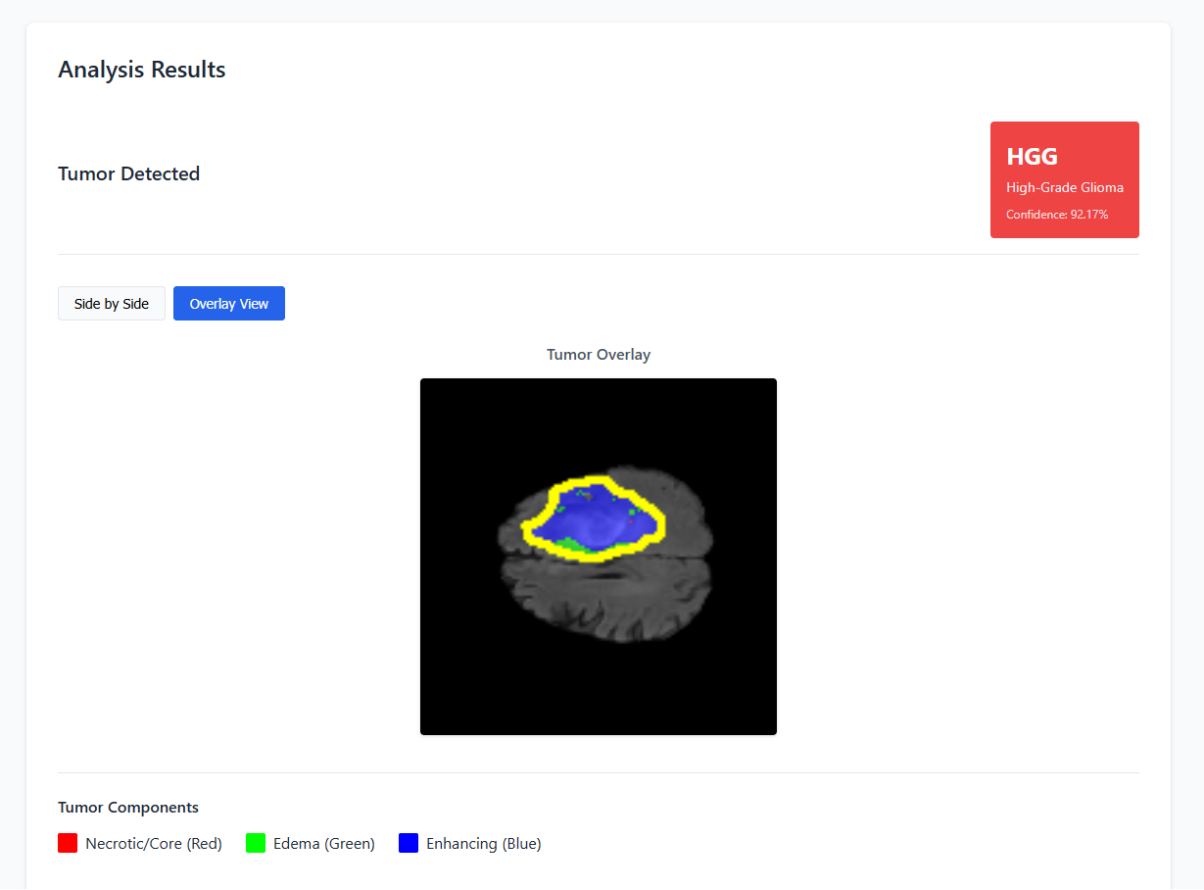

Figure 4.13: Results page of the application demo.

4.7 Conclusion

In this chapter, we have presented a comprehensive methodology for automated brain tumor detection and classification using MR images. Our approach integrates a U-Net-based segmentation model with an SVM classifier, achieving high accuracy and robust performance across multiple evaluation metrics. The segmentation module demonstrated reliable delineation of tumor subregions, while the classification module effectively distinguished between high-grade and low-grade gliomas. Additionally, we showcased the practical application of our framework through a user-friendly demo application, highlighting its potential for real-world clinical use. These contributions underscore the effectiveness of combining deep learning and classical

machine learning techniques in addressing complex medical imaging challenges. Future work could explore further optimization of the pipeline, incorporation of additional data modalities, and validation on larger, more diverse datasets.

General Conclusion

This thesis has explored the development of a hybrid framework for automated brain tumor detection and classification using Magnetic Resonance Imaging (MRI). By integrating deep learning and classical machine learning techniques, we have demonstrated a robust and effective approach to addressing the challenges of brain tumor analysis.

The study began with a comprehensive review of the theoretical foundations, including artificial intelligence, machine learning, and deep learning, with a particular focus on Convolutional Neural Networks (CNNs) and the U-Net architecture. These concepts provided the basis for the segmentation and classification modules of our framework.

The methodology was built upon the BraTS dataset, a benchmark in brain tumor segmentation and classification. We employed a U-Net-based segmentation model to delineate tumor subregions and a Support Vector Machine (SVM) classifier to distinguish between high-grade and low-grade gliomas. The segmentation module achieved an impressive pixel-level accuracy of 99.3%, a mean Intersection over Union (IoU) of 74.66%, and an overall Dice coefficient of 58.98%. These metrics highlight the model's ability to accurately and comprehensively detect tumor regions. The classification module demonstrated strong performance with an overall accuracy of 93.24%.

A key contribution of this work is the integration of these modules into an end-to-end pipeline, capable of processing raw MRI slices to produce segmentation masks and tumor grade predictions. This pipeline was further encapsulated in a user-friendly demo application, showcasing its potential for real-world clinical use.

Despite the promising results, challenges remain. The segmentation module, while accurate, could benefit from further optimization to improve the Dice coefficient and IoU for smaller

tumor subregions. Similarly, the classification module could be enhanced by incorporating additional features or exploring alternative machine learning models. Future work could also focus on expanding the dataset to include more diverse cases, improving generalization across different MRI scanners, and integrating multimodal data for a more comprehensive analysis.

In conclusion, this thesis has demonstrated the feasibility and effectiveness of combining deep learning and classical machine learning techniques for brain tumor analysis. The proposed framework not only advances the state of the art but also lays the groundwork for future research aimed at improving diagnostic accuracy and clinical outcomes in neuro-oncology.

Bibliography

[1] C. Freudenrich, G. J. Tortora, and B. H. Derrickson, *Visualizing Anatomy and Physiology*. Wiley, 2013.

[2] H. Sajedi and N. Pardakhti, "Age prediction based on brain mri image: a survey," *Journal of Medical Systems*, vol. 43, no. 8, pp. 1–30, 2019.

[3] S. Thakkar. (2020, Feb.) Ai vs ml vs dl: What's the difference? Accessed: 2025-05-09. [Online]. Available: https://siddhithakkar.com/2020/02/24/ai-vs-ml-vs-dl-whats-the-difference/

[4] South Jersey Radiology Associates. (2023, Oct.) What should i know about my brain mri results? Consulté le 10 mai 2025. [Online]. Available: https://sjra.com/what-should-i-know-about-my-brain-mri-results/

[5] N. Wiest-Daesslé, "Imagerie du tenseur de diffusion pour l'étude de pathologies cérébrales," Ph.D. dissertation, PhD thesis, Université, 2009.

[6] G. J. Tortora and B. Derrickson, *Manuel d'anatomie et de physiologie humaines*. De Boeck Supérieur, 2017.

[7] N. CHAKRAPARTYJ, "Brain mri images for brain tumor detection," Kaggle dataset, accessed: 2022-01-21. [Online]. Available: https://www.kaggle.com/datasets/navoneel/brain-mri-images-for-brain-tumor-detection

[8] R. Mackenzie, "Gray matter vs white matter," Technology Networks – Neuroscience News and Research, 2019, accessed: 2022-03-21. [Online]. Available: https://www.technologynetworks.com/neuroscience/articles/gray-matter-vs-white-matter-322973

[9] C. Analysis, "MedlinePlus [internet] – bethesda (md): National library of medicine," Online, 2020, accessed: 2022-03-21. [Online]. Available: https://medlineplus.gov/lab-tests/cerebrospinal-fluid-csf-analysis/

[10] D. Slimane, "Segmentation d'image médicale basées sur une coopération fcm et level set," Ph.D. dissertation, Université Mouloud Mammeri, 2015.

[11] M. A. Naser and M. J. Deen, "Brain tumor segmentation and grading of lower-grade glioma using deep learning in mri images," *Computers in Biology and Medicine*, vol. 121, p. 103758, 2020.

[12] T. Armstrong and et al., "Sleep-wake disturbance in patients with brain tumors," *Neuro-oncology*, vol. 19, no. 3, pp. 323–335, 2017.

[13] J. Bittoun, "Basic principles of magnetic resonance imaging," in *SYLLABUS Methodology, Spectroscopy and Clinical MRI*, 1998, pp. 45–52.

[14] Verywell Health, "What you should know about mri," https://www.verywellhealth.com/what-is-an-mri-and-what-does-it-do-3157069, 2023, accessed: 2023-06-05.

[15] S. Bauer, R. Wiest, L. P. Nolte, and M. Reyes, "A survey of MRI-based medical image analysis for brain tumor studies," *Physics in Medicine & Biology*, vol. 58, no. 13, p. R97, 2013.

[16] B. H. Menze, A. Jakab, S. Bauer, J. Kalpathy-Cramer, K. Farahani, J. Kirby *et al.*, "The multimodal brain tumor image segmentation benchmark (BRATS)," *IEEE Transactions on Medical Imaging*, vol. 34, no. 10, pp. 1993–2024, 2015.

[17] S. Bakas, M. Reyes, A. Jakab, S. Bauer, M. Rempfler, A. Crimi *et al.*, "Identifying the best machine learning algorithms for brain tumor segmentation, progression assessment, and overall survival prediction in the BRATS challenge," *arXiv preprint arXiv:1811.02629*, 2018.

[18] L. M. DeAngelis, "Brain tumors," *New England Journal of Medicine*, vol. 344, no. 2, pp. 114–123, 2001.

[19] ScienceDirect Topics, "Artificial intelligence – an overview," https://www.sciencedirect.com/topics/social-sciences/artificial-intelligence, accessed: 2025-04-26.

[20] J. Hurwitz and D. Kirsch, *Machine Learning For Dummies, IBM Limited Edition*. John Wiley & Sons, 2018.

[21] S. R. Gunn, "Support vector machines for classification and regression," 1998. [Online]. Available: https://api.semanticscholar.org/CorpusID:120347962

[22] O. Ronneberger, P. Fischer, and T. Brox, "U-net: Convolutional networks for biomedical image segmentation," in *International Conference on Medical image computing and computer-assisted intervention*. Springer, 2015, pp. 234–241.

[23] S. P. Yadav and S. Yadav, "Image fusion using hybrid methods in multimodality medical images," *Medical & biological engineering & computing*, vol. 58, no. 4, pp. 669–687, 2020.

[24] S. A. Nishu, "Quantifying the defect visibility in digital images by proper color space selection," *International journal of engineering research and applications*, vol. 2, no. 3, pp. 1764–1767, 2012.

[25] R. Yogamangalam, B. Karthikeyan *et al.*, "Segmentation techniques comparison in image processing," *International Journal of Engineering and Technology (IJET)*, vol. 5, no. 1, pp. 307–313, 2013.

[26] M. A. Naser and M. J. Deen, "Brain tumor segmentation and grading of lower-grade glioma using deep learning in mri images," *Computers in Biology and Medicine*, vol. 121, p. 103758, 2020.

[27] S. S. Begum and D. R. Lakshmi, "Combining optimal wavelet statistical texture and recurrent neural network for tumour detection and classification over mri," *Multimedia Tools and Applications*, pp. 1–22, 2020.

[28] R. Hashemzehi, S. J. S. Mahdavi, M. Kheirabadi, and S. R. Kamel, "Detection of brain tumors from mri images base on deep learning using hybrid model cnn and nade," *Biocybernetics and Biomedical Engineering*, vol. 40, no. 3, pp. 1225–1232, 2020.

[29] S. Kulkarni and G. Sundari, "A framework for brain tumor segmentation and classification using deep learning algorithm," *International Journal of Advanced Computer Science and Applications*, vol. 11, 2020.

[30] Z. N. K. Swati, Q. Zhao, M. Kabir, F. Ali, Z. Ali, S. Ahmad, and J. Lu, "Brain tumor classification for mr images using transfer learning and fine-tuning," *Computerized Medical Imaging and Graphics*, vol. 75, pp. 34–46, 2019.